

How Much Should I Trust You?

Modeling Uncertainty of Black Box Explanations

Dylan Slack
University of California, Irvine
dslack@uci.edu

Sophie Hilgard
Harvard University
ash798@g.harvard.edu

Sameer Singh
University of California, Irvine
sameer@uci.edu

Himabindu Lakkaraju
Harvard University
hlakkaraju@seas.harvard.edu

Abstract

As local explanations of black box models are increasingly being employed to establish model credibility in high stakes settings, it is important to ensure that these explanations are accurate and reliable. However, local explanations generated by existing techniques are often prone to high variance. Further, these techniques are computationally inefficient, require significant hyper-parameter tuning, and provide little insight into the quality of the resulting explanations. By identifying lack of uncertainty modeling as the main cause of these challenges, we propose a novel Bayesian framework that produces explanations that go beyond point-wise estimates of feature importance. We instantiate this framework to generate Bayesian versions of LIME and KernelSHAP. In particular, we estimate credible intervals (CIs) that capture the uncertainty associated with each feature importance in local explanations. These credible intervals are tight when we have high confidence in the feature importances of a local explanation. The CIs are also informative both for estimating how many perturbations we need to sample — sampling can proceed until the CIs are sufficiently narrow — and where to sample — sampling in regions with high predictive uncertainty leads to faster convergence. Experimental evaluation with multiple real world datasets and user studies demonstrate the efficacy of our framework and the resulting explanations.

1 Introduction

As machine learning (ML) models are increasingly being deployed in domains such as healthcare and criminal justice, it is important to ensure that decision makers understand these models so that they can diagnose errors and detect model biases correctly. However, ML models that achieve state-of-the-art accuracy are typically complex *black boxes* that are hard to understand. As a consequence, there has been a recent surge in post hoc techniques for explaining black box models [31, 30, 22, 25, 36, 40, 33, 38, 19, 4]. Several of these techniques explain complex black box models by constructing interpretable local approximations such as linear functions (e.g., LIME [30], SHAP [25]) or rules (e.g., MAPLE [28], Anchors [31]), which are much more readily understood by human users. The intuition behind constructing such local approximations is as follows: while complex black box models typically exhibit highly non-linear decision boundaries globally (and are therefore harder to explain *overall*), the behavior of these models tend to be much less complex (e.g., linear decision boundaries) locally, and are therefore more amenable to local explanation.

Existing local explanation methods, however, suffer from serious drawbacks. Explanations generated by methods such as LIME and SHAP are not stable i.e., these explanations vary significantly with

small perturbations to the input that do not change the predictions of the black box model [2, 11, 12, 41, 20]. It has also been empirically demonstrated that multiple runs of these methods on the same instance with the same parameters can result in vastly different explanations [6]. Furthermore, the metrics (e.g., explanation fidelity) that are commonly used to assess the quality of post hoc explanations rely heavily on the internal details of the explanation methods (e.g., the perturbation function used in LIME) and do not provide a true picture of the explanation quality [41]. In addition, there is little to no guidance on how to pick certain hyperparameters that are critical to the quality of the resulting local explanations, e.g., number of perturbed data points to generate. Lastly, these methods are also computationally inefficient because they typically require a large number of model queries to construct local approximations, which is slow for complex neural models.

Contributions We identify the lack of uncertainty modeling as the primary shortcoming of existing post hoc explanation methods. To address the aforementioned drawbacks, we propose a novel Bayesian framework that models the uncertainty associated with local explanations. We instantiate our framework to generate Bayesian versions of LIME and KernelSHAP that not only output point-wise estimates of feature importances but also capture the uncertainty associated with these feature importances by estimating credible intervals (CIs) (see Figure 1 for an example). We compute closed form expressions for the posteriors of our models thereby eliminating the need for any additional computational complexity beyond the original LIME and KernelSHAP methods. The CIs enable us to readily assess the quality of local explanations i.e., explanations with wider CIs may not be sufficiently trustworthy. They are also informative both for estimating how many perturbations we need to sample (until the CIs are sufficiently narrow) and where to sample (regions with high predictive uncertainty), thereby enabling our approaches to be computationally much more efficient in generating accurate local explanations.

We evaluate on a variety of datasets including COMPAS, German Credit, ImageNet, and MNIST. Our results demonstrate the uncertainty estimates produced by our framework are much more reliable proxies of how well the explanation approximates the black box compared to traditional metrics like fidelity. Our experiment results also confirm the correctness of our estimates of the number of perturbations needed to generate explanations of a given level of certainty. Furthermore, proposed uncertainty based sampling speeds up our method by up to a factor of 2 relative to random sampling of perturbations. Lastly, we carry out a user study with 31 humans to evaluate whether explanations generate by our framework focus on important features of the input.

2 Notation & Background

In this section, we establish the necessary notation, discuss the details of two most relevant prior approaches, LIME and SHAP, study the vulnerabilities of these approaches, and illustrate the need for modeling the uncertainty of black box explanations.

Notation Let $f : \mathbb{R}^d \rightarrow [0, 1]$ denote a black box classifier that takes as input a data point x with d features, and returns the probability that x belongs to a certain class $c \in \mathcal{C}$. The goal here is to explain the black box classifier f . Let g denote an explanation that we intend to learn to explain f for instance x , $g \in G$ where G is the class of linear models. We define \mathcal{Z} as a set of N randomly sampled instances (perturbations) around x . The proximity between x and any $z \in \mathcal{Z}$ is given by $\pi_x(z) \in \mathbb{R}$, with a vector over the N perturbations in \mathcal{Z} as $\Pi_x(\mathcal{Z}) \in \mathbb{R}^N$. Let $Y \in \mathbb{R}^N$ be a vector comprising of the black box predictions $f(z)$ corresponding to each of the N instances in \mathcal{Z} .

LIME [30] and **SHAP** [25] are popular *model-agnostic local explanation* approaches that explain individual predictions of any classifier f by learning a linear model g locally around each prediction, where the coefficients of g are treated as the *contribution* of each feature to the corresponding black box prediction. The objective function for both LIME and SHAP is to construct an explanation that

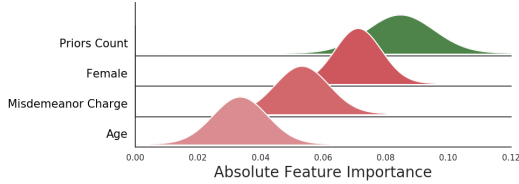
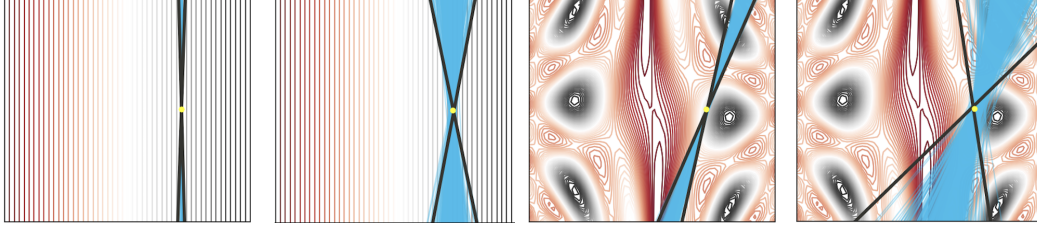


Figure 1: Example explanation from BayesLIME on rearrest prediction in the COMPAS data set. Green indicates features that positively contribute to the prediction while red suggests negative contribution. Our explanation suggests that priors and sex are the most the important features for predicting rearrest. However, our explanation also captures uncertainty about their relative importances.



(a) linear, many samples (b) linear, fewer samples (c) nonlinear, many samples (d) nonlinear, fewer samples

Figure 2: Rerunning LIME local explanations 1000 times and BayesLIME once for linear and non-linear toy surfaces using few (25) and many (250) perturbations. The linear surface is given as $p(y) \propto x_1$ and the non linear surface is defined as $p(y) \propto \sin(x_1/2) * 10 + \cos(10 + (x_1 * x_2)/2) * \cos(x_1)$. We plot each run of LIME in blue and the BayesLIME 95% credible region in black. We see that there is high variance in LIME local explanations and that BayesLIME captures this variance well.

approximates the behavior of the black box accurately in the vicinity (neighborhood) of x , while achieving low complexity $\Omega(g)$ and is thereby interpretable.

$$\arg \min_{g \in \mathcal{G}} L(f, g, \pi_x) + \Omega(g), \quad \text{where loss } L(f, g, \pi_x) = \sum_{z \in \mathcal{Z}} [f(z) - g(z)]^2 \pi_x(z). \quad (1)$$

The main difference between LIME and SHAP lies in how Ω and $\pi_x(z)$ are chosen. In LIME, these are defined heuristically: $\Omega(g)$ is the number of non-zero weights in the linear model g and $\pi_x(z)$ is defined using cosine or l_2 distance. KernelSHAP leverages game theoretic principles to assign values to these functions thereby guaranteeing that the explanations satisfy certain desired properties.

Illustrating Vulnerabilities One of the biggest drawbacks of LIME and KernelSHAP is that the resulting explanations are prone to high variance. We illustrate this phenomenon using a toy 2-dimensional example, and run LIME to explain an instance as we vary the underlying decision surface and number of perturbations, in Figure 2. With a large number of samples and a linear surface in Fig 2a, we see that LIME explanations produced on multiple runs are nearly identical (blue lines), however, reducing the number of samples to 25 results in very different explanations in Fig 2b. For a classifier that violates the linearity assumption, as is common in practice, there is significant variance even with a large number of samples (Fig 2c), with an even wider discrepancy for fewer samples (Fig 2d). For real-world generation of explanations, as we do not know the underlying surface of the classifier and it is not practical to run LIME thousands of times to estimate variance, it is difficult to estimate whether a generated explanation (a single blue line above) is accurate.

3 Bayesian Local Explanations

In this section, we describe our Bayesian framework that is designed to capture the uncertainty associated with local explanations of black box models. First, we discuss the generative process and inference procedure for our Bayesian framework. Then, we highlight how our framework can be instantiated to obtain Bayesian versions of LIME and SHAP. Lastly, we discuss how to construct highly accurate explanations with uncertainty guarantees efficiently using our framework.

3.1 Constructing Bayesian Local Explanations

The goal of this work is two fold: 1) explain the behavior of a given black box model f in the vicinity of a data point x and, 2) model the uncertainty associated with the resulting local explanation. To this end, we propose a novel Bayesian framework for fitting local linear explanations. Our framework is designed to capture two sources of explanation uncertainty: 1) uncertainty associated with the values of the feature importance scores ϕ and, 2) uncertainty associated with how well g captures the local

decision surface of the underlying black box model f . The generative process can be written as:

$$y|z, \phi, \sigma^2 \sim \phi^T z + \underbrace{\mathcal{N}(0, \frac{\sigma^2}{\pi_x(z)})}_{\epsilon} \quad \forall z \in \mathcal{Z} \quad (2)$$

$$\phi|\sigma^2 \sim \mathcal{N}(\phi_0, \sigma^2 \Sigma_0) \quad \sigma^2 \sim \text{Inv-}\chi^2(n_0, \sigma_0^2). \quad (3)$$

Eqn (2) models the linear relationship between the data points $z \in \mathcal{Z}$ and their corresponding black box predictions $y = f(z) \in Y$. We also have an error term $\epsilon \sim \mathcal{N}(0, \frac{\sigma^2}{\pi_x(z)})$ that models the noise in this linear relationship; ϵ captures the error that arises due to the mismatch between our explanation g and the local decision surface of the black box model f . Furthermore, the proximity function $\pi_x(z)$ in this error term ensures that the instances (perturbations) that are in close proximity to the data point x are modeled accurately by the local linear model, while more room for error is allowed for instances that are farther away from x . The conjugate priors on ϕ and σ^2 are shown in Eqn (3). In practice, we set the hyperparameters $\phi_0 = 0$ and $\Sigma_0 = \text{Diag}(1, \dots, 1)$ in order to induce sparsity on ϕ . Additionally, we set n_0 and σ_0^2 to small values (10^{-6}) so that the prior is nearly uninformative.

Inference The posterior distributions on ϕ and σ^2 turn out to be normal and Inv- χ^2 distributions respectively due to the corresponding conjugate priors [27]:

$$\sigma^2|\mathcal{Z}, Y \sim \text{Inv-}\chi^2(N, s^2) \quad \phi|\sigma^2, \mathcal{Z}, Y \sim \text{Normal}(\hat{\phi}, V_\phi \sigma^2) \quad (4)$$

The parameters of these posterior distributions can be computed in closed form:

$$\hat{\phi} = V_\phi \mathcal{Z}^T \text{diag}(\Pi_x(\mathcal{Z})) Y \text{ where } V_\phi = (\mathcal{Z}^T \text{diag}(\Pi_x(\mathcal{Z})) \mathcal{Z} + I)^{-1} \quad (5)$$

$$s^2 = \frac{1}{N} [(Y - \mathcal{Z} \hat{\phi})^T \text{diag}(\Pi_x(\mathcal{Z})) (Y - \mathcal{Z} \hat{\phi}) + \hat{\phi}^T \hat{\phi}] \quad (6)$$

Details of the inference procedure including derivations of Eqns. (4-6) are included in the Appendix.

Estimating Sources of Uncertainty Recall our generative process captures two sources of explanation uncertainty: uncertainty associated with the feature importance scores ϕ , and the uncertainty over the error term ϵ . We assess the former by repeatedly sampling from the posterior distribution of ϕ (Eq (4)). Then, we use these samples to estimate the 95% *credible intervals* of each feature in ϕ . In practice, this term is computed using the 95% density about $\hat{\phi}$ on 10000 samples. We illustrate how these computed intervals capture the variance in the explanations in Figure 2.

The uncertainty over the error term ϵ can be used as a proxy for “explanation quality”, i.e. how well is the explanation accurate to the underlying model. We first calculate the marginal posterior distribution of ϵ by integrating out σ^2 which is given by the Student’s t distribution:

$$\epsilon|\mathcal{Z}, Y \sim t_{(\nu=N)}(0, s^2) \quad (7)$$

To compute our proxy for explanation quality, we evaluate the probability density function (PDF) of this posterior at 0 i.e., $P(\epsilon = 0)$, dropping dependence on \mathcal{Z} and Y for conciseness, to estimate our confidence that there is no error in the explanation. This is computed in closed form using Student’s t and s^2 , which is directly computed from the data. This expression thus gives us the probability density that our explanation g perfectly captures local decision surface of the underlying black box.

Proposition 3.1. *As the number of perturbations sampled around x goes to ∞ i.e., $N \rightarrow \infty$:*

(1) the estimate of ϕ converges to the true importance scores, and its uncertainty converges to 0. (2) uncertainty of the error term ϵ converges to the bias of the local linear model g . [Details in Appendix]

BayesLIME and BayesSHAP We use this framework to generate a Bayesian version of LIME by setting the proximity function to $\pi_x(z) = \exp(-D(x, z)^2/\sigma^2)$ where D is a distance function such as cosine or l_2 distance. This enables us to obtain probabilistic estimates of uncertainty over the LIME feature importances, thereby addressing the some of the drawbacks we discussed in Section 2. Similarly, our framework can also be instantiated to generate a Bayesian version of KernelSHAP by setting $\pi_x(z) = \frac{d-1}{(d \text{ choose } |z|)|z|(d-|z|)}$ where $|z|$ denotes the number of variables in the variable combination represented by the data point z i.e., the number of non-zero valued features in the vector representation of z . Note that the original SHAP method views the problem of constructing a local linear model as estimating the Shapley values corresponding to each of the features [25]. These Shapley values in turn represent the contribution of each of the features to the black box prediction i.e., $f(x) = \phi_0 + \sum \phi_i$. Therefore, the resulting estimates of uncertainty output by BayesSHAP represent how poorly defined the variable contributions are given the current sample of perturbations.

3.2 Estimating Required Number of Perturbations

One of the major drawbacks of previous approaches such as LIME and KernelSHAP is that they do not provide any insight about how to choose the number of perturbations, a key factor in obtaining accurate explanations. We leverage the uncertainty estimates from our framework to compute *perturbations-to-go* (PTG) i.e., how many *more* perturbations are required to obtain explanations that satisfy a desired level of certainty. This estimate thus *predicts* the computational cost of generating an explanation with a desired level of certainty, and can help determine whether it is even worthwhile to do so. The user specifies the confidence level of the CI (denoted as α), and the *maximum* width of the CI (represented as W), e.g. “width of 95% CI interval should be less than 0.1” corresponds to $\alpha = 0.95$ and $W = 0.1$. To estimate PTG for a data point x and its local explanation, we first sample N instances randomly around x (where N is small and chosen by the user) and fit a local linear model using our method as discussed in Section 3.1. This will provide us with initial estimates of various parameters shown in Eqns (4) - (6) which can then be used to compute PTG.

Theorem 3.2. *Given N seed perturbations, the number of additional perturbations required, PTG, to achieve a credible interval width W of feature importance for a given data point x at user-specified confidence level α can be computed as:*

$$PTG(W, \alpha, x) = \frac{4s_N^2}{\bar{\pi}_N \times \left[\frac{W}{\Phi^{-1}(\alpha)} \right]^2} - N \quad (8)$$

where $\bar{\pi}_N$ is the average proximity $\pi_x(z)$ for the N perturbations, s_N^2 is the empirical sum of squared errors (SSE) between the black box and local linear model predictions, weighted by $\pi_x(z)$, as in (6), and $\Phi^{-1}(\alpha)$ is the two-tailed inverse normal CDF at confidence level α .

Proof (Sketch). To estimate PTG, we first relate W and α to $\text{Var}(\phi_i)$, variance of the marginal importance distribution for any feature i , obtained by integrating out σ^2 .¹ Because Student’s t can be approximated by a Normal distribution for large degrees of freedom (here, N should be large enough), we use the inverse normal CDF to calculate CI width at level α . We then compute V_ϕ from (5) using \mathcal{Z} , treating its entries as Bernoulli distributed with probability 0.5. Due to the covariance structure of this sampling procedure, the resulting variance estimate after S samples is the sample SSE s_N^2 scaled by $\approx \frac{4}{\bar{\pi}_N S}$ (full derivation included in the Appendix C). If we assume SSE scales linearly with N , we can take this to be a reasonable estimate of s_S^2 at any S . We can then estimate PTG

$$\left[\frac{W}{\Phi^{-1}(\alpha)} \right]^2 = \text{Var}(\phi_i) = \frac{4s_N^2}{\bar{\pi}_N \times S} \Rightarrow S = \frac{4s_N^2}{\bar{\pi}_N \times \left[\frac{W}{\Phi^{-1}(\alpha)} \right]^2} \Rightarrow PTG = \frac{4s_N^2}{\bar{\pi}_N \times \left[\frac{W}{\Phi^{-1}(\alpha)} \right]^2} - N \quad (9)$$

□

3.3 Efficient Construction of Bayesian Local Explanations

So far, we have provided methods to estimate uncertainty in explanations and compute how many perturbations are needed to achieve a desired level of certainty. However, if PTG is large, generating explanations by querying the black-box model for labels of a large number of perturbations can be computationally expensive especially in case of complex models such as deep neural networks [8, 17]. In this section, we propose an alternative approach to querying the black-box model that is more targeted than querying randomly (as existing approaches do). Inspired by active learning [34], we introduce a batch-sampling procedure called *uncertainty sampling* that strategically prioritizes perturbations whose predictions we are most uncertain about. Specifically, we compute the posterior predictive distribution for any new instance z :

$$\hat{y}(z) | \mathcal{Z}, Y \sim t_{(V=N)}(\hat{\phi}^T z, (z^T V_\phi z + 1)s^2) \quad (10)$$

¹Note that the value of $\text{Var}(\phi_i)$, the marginal variance of the feature importance for feature i obtained by integrating out σ^2 , is similar for all features. This is due to the fact that this variance captures random error which is a function of the number of perturbations and is therefore common across all features.

Data set	BayesLIME	BayesSHAP
ImageNet	94.8	89.9
MNIST	97.2	90.1
COMPAS	95.5	87.9
German Credit	96.9	89.6

Figure 3: Assessing BayesLIME and BayesSHAP credible intervals. We report the % of time the 95% credible intervals with 100 perturbations include their true values (estimated on 10,000 perturbations). Closer to 95.0 is better.

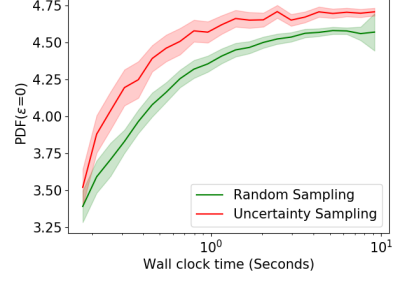


Figure 4: Mean and std error of the explanation quality (y-axis) over time with different query strategies, for 100 Imagenet images.

The variance of the aforementioned student’s t distribution is $((z^T V_\phi z + 1)s^2)(N/(N - 2))$, which we refer to as *predictive variance* captures how uncertain g is about the black box label for an instance z . We prioritize querying the black box model with perturbations that have high predictive variance.

Our uncertainty sampling procedure proceeds as follows: 1) We first randomly sample N instances (perturbations) around the data point x . Let us call this set \mathcal{Q} . 2) We then compute $\exp(z^T V_\phi z + 1)s^2 / \sum_{z \in \mathcal{Q}} \exp(z^T V_\phi z + 1)s^2$ for each perturbation $z \in \mathcal{Q}$ thereby generating a distribution over all the points in \mathcal{Q} . Let us call this resulting distribution \mathcal{Q}_{dist} . 3) We then draw B perturbations from \mathcal{Q}_{dist} and query the black box model for labels of these B instances. 4) Using the newly sampled B instances as well as the N initial perturbations and their corresponding black box labels, we fit a local linear model g as discussed in Section 3.1. 5) If the resulting explanation satisfies the desired level of certainty, terminate early and return the local explanation, otherwise, repeat steps (1) - (5). In practice, we observe that this procedure allows us to obtain explanations with desired levels of certainty with far fewer than PTG number of queries to the black box. Pseudocode for this procedure is provided in the Appendix.

4 Experiments

We evaluate the proposed framework by first analyzing the quality of the uncertainty estimates output by our framework for both feature importances and error. Next, we assess the correctness of our estimates of required perturbations (*PTG*), and evaluate the computational efficiency of our uncertainty based sampling procedure. Last, we describe a user study that we carried out with 31 human subjects to assess the informativeness of the explanations output by our framework.

Setup We experiment with a variety of real world datasets spanning multiple applications (e.g., criminal justice and credit scoring) as well as modalities (e.g., structured data, images). Our first structured dataset is **COMPAS** [3], containing criminal history, jail and prison time, and demographic attributes of 6172 defendants, with class labels that represent whether each defendant was rearrested within 2 years of release. The second structured dataset is the **German Credit** dataset from the UCI repository [9] containing financial and demographic information (including account information, credit history, employment, gender) for 1000 loan applications, each labeled as a “good” or “bad” customer. We create 80/20 train/test splits for these two datasets, and train a random forest classifier (sklearn implementation with 100 estimators) as *black box* models for each (test accuracy of 62.5% and 64.0%, respectively). We also include popular image datasets—MNIST and Imagenet. For the **MNIST** [23] handwritten digits dataset, we train a 2-layer CNN to predict the digits (test accuracy of 99.2%) and use the prediction of digit “4” as the target class. For **Imagenet** [7], we use the off-the-shelf VGG16 model [35] as the black box, and select a sample of 100 “French bulldog” images as our test set and explanation target (the model predicts French bulldog on 88% of these images). For generating explanations, we use standard implementations of the baselines LIME and KernelSHAP with default settings [30, 26]. For images, we construct super pixels as described in Ribeiro et al. [30] and use them as the features to use in the explanation (number of super pixels is fixed to 20 per image). For our framework, we set perturbation sample size $N = 50$, batch size $B = 10$, and the desired level of certainty is expressed as the width of the 95% credible interval.

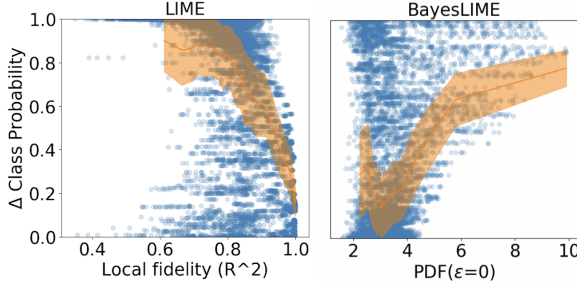


Figure 5: Δ class probability when top 5% of super pixels using LIME fidelity and BayesLIME $\text{PDF}(\epsilon = 0)$ are masked, with different perturbation sizes & 1,000 images (mean and std deviation in orange). $\text{PDF}(\epsilon = 0)$ has a *positive relationship* with the explanation quality while fidelity has *negative*; both significant as per Pearson’s r test ($p < 10^{-20}$).

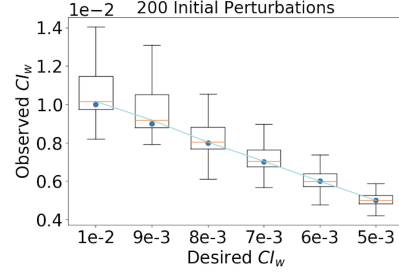


Figure 6: Desired versus observed CI_w running on the PTG estimate. We consider different desired certainty levels and 100 MNIST images. PTG is estimated from 200 initial samples from the classifier (varies between 200 and 20000 across images).

Quality of Uncertainty Estimates The key component of our explanations are the estimates of uncertainty (CIs) associated with the feature importances. To evaluate the correctness of these estimates, we compute how often *true* feature importances lie within the 95% credible intervals estimated by BayesLIME and BayesSHAP. We evaluate the quality of the CI estimates by running our methods with 100 perturbations to estimate feature importances and corresponding 95% CIs for each test instance, and computing what fraction of the true feature importances fall within our 95% CI estimates. Since we do not have access to the true feature importances of the complex black box models, following Prop 3.1, we use feature important computed from a large value of N ($N = 10000$), and treat the resulting estimates as ground truth. Results for BayesLIME in Table 3 indicate that the true feature importances fall within estimated CIs about 94.8% to 97.2% of the time, confirming that these uncertainty estimates are very well calibrated. While the estimates by BayesSHAP are somewhat less calibrated (true feature importances fall within our estimated 95% CIs about 89.6 to 90.1% of the time), this may be due to the previously known drawback that the Shapley kernel produce extremely small proximity scores for perturbations [25], leading to instabilities in uncertainty estimation. All in all, these results confirm that the CIs learned by our methods are well calibrated and therefore highly reliable in capturing the uncertainty of the feature importances.

Explanation Error as a Metric of Explanation Quality Recall that $P(\epsilon = 0)$ (Eqn. 7) gives us the probability density that an explanation perfectly captures the local decision surface of the underlying black box, and can therefore be used to evaluate the quality of explanations. Here, we assess if this notion of explanation quality is more reliable than another commonly used metric – locally weighted R^2 (local fidelity) [41, 30]. To this end, we use Δ class-probability [16, 13], which is defined as $f(x) - f(x')$ and corresponds to the change in the probability output by the black box model f as we go from an instance x to another instance x' . To illustrate how this metric can be used to compare explanation quality, consider two local linear models g and g' that approximate f around an image x . If g is a better explanation than g' , removing the most important features highlighted by g from image x should result in a larger change in the Δ class-probability than removing the most important features highlighted by g' . We compare how explanations ranked using $\text{PDF}(\epsilon = 0)$ and fidelity compare to Δ class-probability, with higher correlation indicating a better metric for explanation quality. We take every image x in the MNIST test set, identify its top 5% most important features using our estimates of $\hat{\phi}$, mask these features to obtain a new image x' , and measure the corresponding Δ class-probability, as well as the evaluation metrics $\text{PDF}(\epsilon = 0)$ for BayesLIME/BayesSHAP and local fidelity in case of LIME/SHAP. We repeat this varying number of perturbations, and show scatter plots of evaluation metrics vs. Δ class-probability in Figure 5 (results for SHAP and BayesSHAP are in Appendix). Δ class-probability has a *negative* relationship with local fidelity while it has a clear *positive* relationship with our metric $P(\epsilon = 0)$. This may be because local fidelity does not account for perturbation sample size i.e., an explanation with a weighted R^2 of 0.9 learned using 10 perturbations is considered better than another explanation with a weighted R^2 of 0.85 learned using 10000 perturbations. These results clearly demonstrate that our metric $P(\epsilon = 0)$ is much more reliable than local fidelity in evaluating the quality of explanations.

Correctness of the Estimated Number of Perturbations We assess whether our estimate of *perturbations-to-go* (PTG) is an accurate estimate of the *additional* number of perturbations needed to reach a desired level of feature importance certainty. We carry out this experiment on MNIST data and use $N = 200$ as the initial number of perturbations to obtain a preliminary explanation and its associated uncertainty estimates. We then leverage these estimates to compute PTG for 6 different certainty levels. For each image and certainty level, we run our method for the estimated number of perturbations (PTG) to determine if the resulting certainty levels (observed CI_w) match the corresponding desired levels of certainty (desired CI_w). Results in Figure 6 show that the observed and desired levels of certainty are well calibrated demonstrating that PTG estimates are reliable approximations of the additional number of perturbations needed. We also observed significant differences in PTG estimates across instances (details in Appendix) i.e. number of perturbations needed to obtain explanations with a particular level of certainty varied significantly across instances—ranging from 200 – 5000 for the lowest level of certainty to 200 – 20000 for higher levels of certainty.

Efficiency of Uncertainty Sampling Recall that our *uncertainty sampling* procedure in Section 3.2 uses the *predictive variance* to strategically choose perturbations which will reduce uncertainty in order to be labeled by the black box. Here, we evaluate whether uncertainty sampling produces higher quality explanations (measured by $P(\epsilon = 0)$) more efficiently than random sampling. We experiment with BayesLIME on Imagenet data to carry out this analysis. This setting replicates real-world scenarios where LIME is not preferred as it is computationally expensive to query complex black boxes (e.g., VGG16). We run each sampling strategy for 10 seconds and plot wall clock time (computed on a machine with an Intel Core i9-9900 CPU) vs. explanation quality ($P(\epsilon = 0)$). Results in Figure 4 show that uncertainty sampling results in faster convergence to high quality explanations compared to random sampling; uncertainty sampling also stabilizes within a few seconds where as random sampling takes closer to 10 seconds. Results with number of model queries vs. explanation quality are included in Appendix D. These results clearly demonstrate that uncertainty sampling can significantly speedup the process of generating high quality local explanations.

User Study We perform a user study to compare BayesLIME and LIME explanations on MNIST. We evaluate the following: are more confident explanations more meaningful for humans? To evaluate this question, we mask the most important features selected by BayesLIME and LIME, and ask users to determine the class. The better the explanation, the more difficult it should be for the users to guess the right digit. We randomly select 15 correctly predicted images from the MNIST test set, generate explanations by sweeping over the same perturbation sizes as Figure 5, and choose the *top* explanation for each image by either fidelity (for LIME) or $P(\epsilon = 0)$ (for BayesLIME). We mask the top 3 features from each image and ask 31 users to determine the correct digit for all the images (example of the interface included in Figure 11 Appendix E). We find that the explanations identified by our method focus on more useful parts of the image for humans, since hiding them makes it difficult to guess the digit. Users had an error rate for LIME of 25.7%, while it was 30.7% for BayesLIME, both with standard error 0.003 ($\rho = 0.028$ through a one-tailed two sample t-test).

5 Discussion & Conclusion

We propose a novel Bayesian framework that models the uncertainty associated with local explanations. The uncertainty estimates in the form of credible intervals (CIs) output by our framework are not only informative in assessing the quality of local explanations, but also in estimating critical hyperparameters and making the process of learning local explanations highly efficient. While some prior work has attempted to tackle the problem of modeling uncertainty in the context of explanations either by averaging over several explanations [43, 24] or adopting a Bayesian non-parametric approach [14], these methods are prohibitively expensive in terms of computation. We achieve similar outcomes with minimal computational overhead. Furthermore, our method additionally provides useful information regarding where and how much to sample to reduce sampling uncertainty efficiently.

Quantifications of explanation uncertainty [32], along with the development of sanity checks for explainers [5, 1, 42], represent an important step to improved usability given experimental evidence that humans are often too eager to accept inaccurate machine explanations [18, 15, 29, 21]. Our contribution paves the way for future work measuring other sources of uncertainty in explanations and exploring how this uncertainty quantification can reduce errors of algorithmic overconfidence in domains such as healthcare, criminal justice, and business.

Broader Impact

Interpretability of complex black box models in machine learning is a quickly growing area of research with immediate societal considerations. Our work addresses issues of explanation methods unreliability through better expressing notions of explanation uncertainty. This method could better allow users to understand whether they have generated reliable, replicable model explanations. In particular, it could provide guidelines for when *not to* trust any given explanation. Such endeavors could have positive downstream societal outcomes through mitigating the effects of faulty model explanations, and open up potential applications domains for interpretable machine learning.

Though this methods presents potential societal upsides, there are potential negative outcomes considering the context and use case of the method. The primary concern we see is that users could potentially conflate low sampling uncertainty with unrelated sources of uncertainty, in particular model uncertainty. This may exacerbate the effect of explanations leading to justification and overtrust of inaccurate model predictions [18, 15, 29]. Furthermore, our method identifies only *sample uncertainty* for a fixed perturbation distribution and so does not protect against adversarial attacks on explanation methods which leverage gaps between the data distribution and the perturbation distribution [37]. Mitigating the above concerns will require broader initiatives to educate users around the specific use cases and failings of explanation methods [39] as well as interdisciplinary efforts with social psychologists and HCI practitioners to make the potential errors of explanation methods more salient.

References

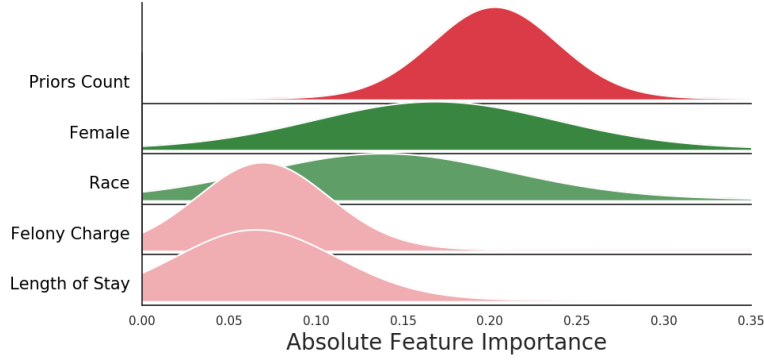
- [1] Julius Adebayo, Justin Gilmer, Michael Muelly, Ian Goodfellow, Moritz Hardt, and Been Kim. Sanity checks for saliency maps. In *Advances in Neural Information Processing Systems*, pages 9505–9515, 2018.
- [2] David Alvarez-Melis and Tommi S. Jaakkola. On the robustness of interpretability methods. *ICML Workshop on Human Interpretability in Machine Learning*, 2018.
- [3] Julia Angwin, Jeff Larson, Surya Mattu, and Lauren Kirchner. Machine bias. In *ProPublica*, 2016.
- [4] Osbert Bastani, Carolyn Kim, and Hamsa Bastani. Interpretability via model extraction. *FAT/ML Workshop 2017*, 2017.
- [5] Oana-Maria Camburu, Eleonora Giunchiglia, Jakob Foerster, Thomas Lukasiewicz, and Phil Blunsom. Can i trust the explainer? verifying post-hoc explanatory methods. *arXiv preprint arXiv:1910.02065*, 2019.
- [6] Jianbo Chen, Le Song, Martin J. Wainwright, and Michael I. Jordan. L-shapley and c-shapley: Efficient model interpretation for structured data. In *International Conference on Learning Representations*, 2019.
- [7] J. Deng, W. Dong, R. Socher, L.-J. Li, K. Li, and L. Fei-Fei. ImageNet: A Large-Scale Hierarchical Image Database. In *CVPR09*, 2009.
- [8] Emily L. Denton, Wojciech Zaremba, Joan Bruna, Yann LeCun, and Rob Fergus. Exploiting linear structure within convolutional networks for efficient evaluation. In *NIPS*, 2014.
- [9] Dheeru Dua and Casey Graff. Uci machine learning repository, 2017. URL <http://archive.ics.uci.edu/ml>.
- [10] Ludwig Fahrmeir, Thomas Kneib, and Stefan Lang. *Regression*. Statistik und ihre Anwendungen. Springer, Berlin [u.a.], 2007. ISBN 978-3-540-33932-8. URL http://gso.gbv.de/DB=2.1/CMD?ACT=SRCHA&SRT=YOP&IKT=1016&TRM=ppn+510939260&sourceid=fwb_bibsonomy.
- [11] Amirata Ghorbani, Abubakar Abid, and James Zou. Interpretation of neural networks is fragile. In *Proceedings of the AAAI Conference on Artificial Intelligence*, volume 33, pages 3681–3688, 2019.

- [12] Sebastian Gruber and Christoph Molnar. *LIME and Sampling*. URL https://compstat-lmu.github.io/iml_methods_limitations/lime-sample.html.
- [13] Jindong Gu, Yinchong Yang, and Volker Tresp. Understanding individual decisions of cnns via contrastive backpropagation. In *Asian Conference on Computer Vision*, pages 119–134, 05 2019. ISBN 978-3-030-20892-9. doi: 10.1007/978-3-030-20893-6_8.
- [14] Wenbo Guo, Sui Huang, Yunzhe Tao, Xinyu Xing, and Lin Lin. Explaining deep learning models – a bayesian non-parametric approach. In S. Bengio, H. Wallach, H. Larochelle, K. Grauman, N. Cesa-Bianchi, and R. Garnett, editors, *Advances in Neural Information Processing Systems 31*, pages 4514–4524. Curran Associates, Inc., 2018. URL <http://papers.nips.cc/paper/7703-explaining-deep-learning-models-a-bayesian-non-parametric-approach.pdf>.
- [15] Fred Hohman, Andrew Head, Rich Caruana, Robert DeLine, and Steven M Drucker. Gamut: A design probe to understand how data scientists understand machine learning models. In *Proceedings of the 2019 CHI Conference on Human Factors in Computing Systems*, pages 1–13, 2019.
- [16] Brian Iwana, Ryohei Kuroki, and Seiichi Uchida. Explaining convolutional neural networks using softmax gradient layer-wise relevance propagation. In *IEEE/CVF International Conference on Computer Vision Workshop*, pages 4176–4185, 10 2019.
- [17] Max Jaderberg, Andrea Vedaldi, and Andrew Zisserman. Speeding up convolutional neural networks with low rank expansions. *BMVC 2014 - Proceedings of the British Machine Vision Conference 2014*, 05 2014. doi: 10.5244/C.28.88.
- [18] Harmanpreet Kaur, Harsha Nori, Samuel Jenkins, Rich Caruana, Hanna Wallach, and Jennifer Wortman Vaughan. Interpreting interpretability: Understanding data scientists’ use of interpretability tools for machine learning. In *CHI 2020*, April 2020.
- [19] Pang Wei Koh and Percy Liang. Understanding black-box predictions via influence functions. In *Proceedings of the 34th International Conference on Machine Learning-Volume 70*, pages 1885–1894. JMLR. org, 2017.
- [20] I Elizabeth Kumar, Suresh Venkatasubramanian, Carlos Scheidegger, and Sorelle Friedler. Problems with shapley-value-based explanations as feature importance measures. *International Conference on Machine Learning*, Forthcoming 2020.
- [21] Himabindu Lakkaraju and Osbert Bastani. "how do i fool you?" manipulating user trust via misleading black box explanations. In *Proceedings of the AAAI/ACM Conference on AI, Ethics, and Society*, pages 79–85, 2020.
- [22] Himabindu Lakkaraju, Ece Kamar, Rich Caruana, and Jure Leskovec. Faithful and customizable explanations of black box models. In *Proceedings of the 2019 AAAI/ACM Conference on AI, Ethics, and Society*, pages 131–138. ACM, 2019.
- [23] Yann LeCun, Corinna Cortes, and CJ Burges. Mnist handwritten digit database. *ATT Labs [Online]*. Available: <http://yann.lecun.com/exdb/mnist>, 2, 2010.
- [24] Eunjin Lee, David Braines, Mitchell Stiffler, Adam Hudler, and Daniel Harborne. Developing the sensitivity of lime for better machine learning explanation. In *Artificial Intelligence and Machine Learning for Multi-Domain Operations Applications*, volume 11006, page 1100610. International Society for Optics and Photonics, 2019.
- [25] Scott M Lundberg and Su-In Lee. A unified approach to interpreting model predictions. In *Advances in Neural Information Processing Systems*, pages 4765–4774, 2017.
- [26] Scott M Lundberg and Su-In Lee. A unified approach to interpreting model predictions. In I. Guyon, U. V. Luxburg, S. Bengio, H. Wallach, R. Fergus, S. Vishwanathan, and R. Garnett, editors, *Advances in Neural Information Processing Systems 30*, pages 4765–4774. Curran Associates, Inc., 2017. URL <http://papers.nips.cc/paper/7062-a-unified-approach-to-interpreting-model-predictions.pdf>.

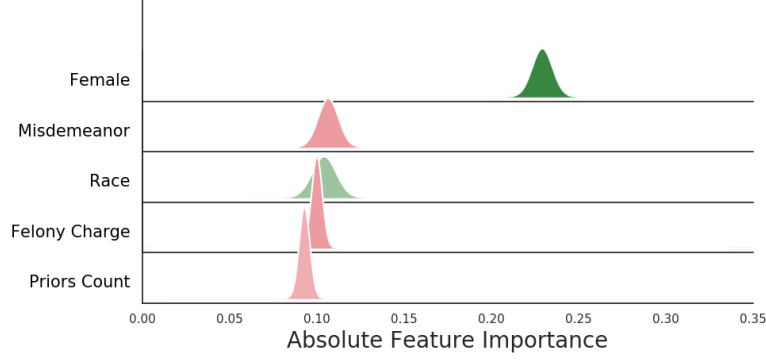
- [27] Andrew Moore. Locally weighted bayesian regression, January 1995.
- [28] Gregory Plumb, Denali Molitor, and Ameet S Talwalkar. Model agnostic supervised local explanations. In *Advances in Neural Information Processing Systems*, pages 2515–2524, 2018.
- [29] Forough Poursabzi-Sangdeh, Daniel G Goldstein, Jake M Hofman, Jennifer Wortman Vaughan, and Hanna Wallach. Manipulating and measuring model interpretability. *arXiv preprint arXiv:1802.07810*, 2018.
- [30] Marco Tulio Ribeiro, Sameer Singh, and Carlos Guestrin. " why should i trust you?" explaining the predictions of any classifier. In *Proceedings of the 22nd ACM SIGKDD international conference on knowledge discovery and data mining*, pages 1135–1144, 2016.
- [31] Marco Tulio Ribeiro, Sameer Singh, and Carlos Guestrin. Anchors: High-precision model-agnostic explanations. In *Thirty-Second AAAI Conference on Artificial Intelligence*, 2018.
- [32] Patrick Schwab and Walter Karlen. Cxplain: Causal explanations for model interpretation under uncertainty. In H. Wallach, H. Larochelle, A. Beygelzimer, F. d'Alché-Buc, E. Fox, and R. Garnett, editors, *Advances in Neural Information Processing Systems 32*, pages 10220–10230. Curran Associates, Inc., 2019. URL <http://papers.nips.cc/paper/9211-cxplain-causal-explanations-for-model-interpretation-under-uncertainty.pdf>.
- [33] Ramprasaath R Selvaraju, Michael Cogswell, Abhishek Das, Ramakrishna Vedantam, Devi Parikh, and Dhruv Batra. Grad-cam: Visual explanations from deep networks via gradient-based localization. In *Proceedings of the IEEE international conference on computer vision*, pages 618–626, 2017.
- [34] Burr Settles. Active learning literature survey. 2010.
- [35] Karen Simonyan and Andrew Zisserman. Very deep convolutional networks for large-scale image recognition. In *International Conference on Learning Representations*, 2015.
- [36] Karen Simonyan, Andrea Vedaldi, and Andrew Zisserman. Deep inside convolutional networks: Visualising image classification models and saliency maps. In *Workshop at International Conference on Learning Representations*, 2014.
- [37] Dylan Slack, Sophie Hilgard, Emily Jia, Sameer Singh, and Himabindu Lakkaraju. Fooling lime and shap: Adversarial attacks on post hoc explanation methods. *AAAI/ACM Conference on Artificial Intelligence, Ethics, and Society (AIES)*, 2020.
- [38] Daniel Smilkov, Nikhil Thorat, Been Kim, Fernanda Viégas, and Martin Wattenberg. Smoothgrad: removing noise by adding noise. *Workshop on Visualization for Deep Learning, ICML*, 2017.
- [39] Kacper Sokol and Peter Flach. Explainability fact sheets: a framework for systematic assessment of explainable approaches. In *Proceedings of the 2020 Conference on Fairness, Accountability, and Transparency*, pages 56–67, 2020.
- [40] Mukund Sundararajan, Ankur Taly, and Qiqi Yan. Axiomatic attribution for deep networks. In *Proceedings of the 34th International Conference on Machine Learning-Volume 70*, pages 3319–3328. JMLR. org, 2017.
- [41] Hui Fen Tan, Kuangyan Song, Madeilene Udell, Yiming Sun, and Yujia Zhang. “why should you trust my explanation?” understanding uncertainty in lime explanations. In *ICML Workshop on AI for Social Good*, 2019.
- [42] Mengjiao Yang and Been Kim. Bim: Towards quantitative evaluation of interpretability methods with ground truth. *arXiv preprint arXiv:1907.09701*, 2019.
- [43] Chih-Kuan Yeh, Cheng-Yu Hsieh, Arun Suggala, David I Inouye, and Pradeep K Ravikumar. On the (in) fidelity and sensitivity of explanations. In *Advances in Neural Information Processing Systems*, pages 10965–10976, 2019.

A BayesLIME Case Study

We consider two explanations output by our method BayesLIME to explain a random forest classifier (black box) trained on the COMPAS dataset. One of these explanations is generated using fewer perturbations (100), and the other is generated using larger number of perturbations (5000). Figures 7 & 8 show the top 5 features corresponding to each of these explanations, the associated feature importance distributions. In case of few perturbations, BayesLIME suggests that the true feature importance values could vary significantly from the mean estimates. With several perturbations, the feature importances are much more certain. Additionally, the importance ranking amongst the features has changed significantly. `sex` turns out to be the most important feature while `priors count` has dropped in relative importance. Though the feature importances change significantly with additional perturbations, BayesLIME correctly captures this uncertainty even with fewer perturbations.



(a) Explanations learned using 100 perturbations. Top 5 features (priors count being the most important) and their corresponding feature importance distributions.



(b) Explanations learned using 5000 perturbations. Top 5 features (sex being the most important) and their corresponding feature importance distributions.

B Model derivation

B.1 Derivation of posterior

From the assumption that σ^2 is uninformative, namely that the prior parameters are about 0, we write the joint posterior as

$$\phi, \sigma^2 | Y, Z \propto \rho(Y|X, \beta, \sigma^2) \rho(\beta|\sigma^2) \rho(\sigma^2) \quad (11)$$

$$\propto (\sigma^2)^{-N/2} \exp\left(-\frac{1}{2\sigma^2} (Y - Z\phi)^T \text{diag}(\Pi_x(Z)) (Y - Z\phi)\right) (\sigma^2)^{-1} \exp\left(-\frac{1}{2\sigma^2} \phi^T \phi\right) \quad (12)$$

Letting $\hat{\phi} = (\mathcal{Z}^T \text{diag}(\Pi_x(\mathcal{Z}))\mathcal{Z} + I)^{-1} \mathcal{Z}^T \text{diag}(\Pi_x(\mathcal{Z}))Y$, we group terms in the exponentials according to ϕ . The intermediate steps can be found in [10].

$$= (Y - X\phi)^T \text{diag}(\Pi_x(\mathcal{Z}))(Y - X\phi) + \phi^T \phi \quad (13)$$

$$= [\phi - \hat{\phi}]^T (\mathcal{Z}^T \text{diag}(\Pi_x(\mathcal{Z}))\mathcal{Z} + I)[\phi - \hat{\phi}] \quad (14)$$

Using what we've derived so far, we can write down the conditional posterior of ϕ as

$$\phi|\sigma^2, Y, \mathcal{Z} \propto \exp\left(\frac{1}{2}\sigma^{-2}[\phi - \hat{\phi}]^T (\mathcal{Z}^T \text{diag}(\Pi_x(\mathcal{Z}))\mathcal{Z} + I)[\phi - \hat{\phi}]\right) \quad (15)$$

So, we can see that our estimates for the mean and variance of $\rho(\phi|\sigma^2, Y, \mathcal{Z})$ are $\hat{\phi}$ and $\sigma^2(\mathcal{Z}^T \text{diag}(\Pi_x(\mathcal{Z}))\mathcal{Z} + I)^{-1}$.

Next, we derive the conditional posterior for σ^2 . We identify the form of the scaled inverse- χ^2 distribution in the joint posterior as in [27] and write

$$\sigma^2|\mathcal{Z}, \hat{\phi}, Y \sim \text{Inv-}\chi^2(N, s^2) \quad (16)$$

where

$$s^2 = \frac{(y - \mathcal{Z}\hat{\phi})^T \text{diag}(\Pi_x(\mathcal{Z}))(y - \mathcal{Z}\hat{\phi}) + \hat{\phi}^T \hat{\phi}}{N} \quad (17)$$

B.2 Derivation of equations (7) & (10)

We first establish the identity $\sigma^2 \sim \text{Inv-}\chi^2(a, b)$ and $z|\sigma^2 \sim \mathcal{N}(\mu, \lambda\sigma^2) \iff z \sim t_{(v=a)}(\mu, \lambda b)$ [27].

(7) We have, $\epsilon \sim \mathcal{N}(0, \sigma^2)$, $\sigma^2 \sim \text{Inv-}\chi^2(N, s^2)$. Then, it's the case that $\epsilon \sim t_{(v=N)}(0, s^2)$.

(10) We have $\hat{y} \sim \hat{\phi}^T z + \epsilon$ for some z . Thus, $\hat{y} \sim \mathcal{N}(\hat{\phi}^T z, z^T V_{\phi} z \sigma^2) + \mathcal{N}(0, \sigma^2)$, where $\sigma^2 \sim \text{Inv-}\chi^2(N, s^2)$. So, we have $\hat{y} \sim t_{v=N}(\hat{\phi}^T z, (z^T V_{\phi} z + 1)s^2)$.

C Proof of Theorems

In this appendix, we prove proposition 3.1 and theorem 3.2.

In these derivations, the perturbation matrices \mathcal{Z} have elements $\mathcal{Z}_{ij} \in \{0, 1\}$ where each $\mathcal{Z}_{ij} \sim \text{Bernoulli}(0.5)$. This convention is typically used to denote features being ‘‘included’’ (1) or ‘‘excluded’’ (0) [30, 26].

We initially prove theorem 3.2 because the results contained in this proof are useful for the propositions.

C.1 Proof of Theorem 3.2

We use three assumptions stated as follows. First, $\frac{\pi S}{2}$ is sufficiently large such that $\frac{\pi S}{2} + 1$ is equivalent to $\frac{\pi S}{2}$. Second, S is sufficiently large such that $S + 1$ is equivalent to S and $\frac{S}{S-2}$ is equivalent to 1. Third, the product of $\mathcal{Z}^T \text{diag}(\Pi_x(\mathcal{Z}))\mathcal{Z}$ within V_{ϕ} can be taken at its expected value.

Note that we use S to denote the *total* perturbations while we use N to denote the perturbations collected *so far*.

First, we state the marginal distribution over feature importance ϕ_i where i is an arbitrary feature importance $i \in d$. This given as

$$\phi_i | \mathcal{Z}, Y \sim t_{\mathcal{V}=N}(\hat{\phi}_i, V_{\phi_{ii}} s^2) \quad (18)$$

where $V_\phi = (\mathcal{Z}^T \text{diag}(\Pi_x(\mathcal{Z})) \mathcal{Z} + I)^{-1}$. Recalling each element of \mathcal{Z} , i.e. \mathcal{Z}_{ij} , is given $\sim \text{Bern}(.5)$ we use the third assumption to write V_ϕ

$$V_\phi = \begin{bmatrix} \frac{\pi S}{2} + 1 & \frac{\pi S}{4} & \cdots \\ \frac{\pi S}{4} & \ddots & \\ \vdots & & \frac{\pi S}{2} + 1 \end{bmatrix}^{-1} \quad (19)$$

We can see this is the case considering that each element in \mathcal{Z} is a $\text{Bern}(.5)$ draw. So, the diagonals are scaled by $S/2$ because these are the expected value of the dot product of each row with itself. The off-diagonals are scaled by $S/4$ considering this is expected value of the dot product of a row with a row besides itself. Dropping 1's due the first assumption

$$V_\phi = \begin{bmatrix} \frac{\pi S}{2} & \frac{\pi S}{4} & \cdots \\ \frac{\pi S}{4} & \ddots & \\ \vdots & & \frac{\pi S}{2} \end{bmatrix}^{-1} \quad (20)$$

where $\frac{\pi S}{2}$ defines the diagonal and $\frac{\pi S}{4}$ defines the off diagonal elements. Through the Sherman-Morrison formula, we can write the inverse of this matrix as

$$V_\phi = \left[\begin{bmatrix} \frac{\pi S}{2} - \frac{\pi S}{4} & 0 & \cdots \\ 0 & \ddots & \\ \vdots & & \frac{\pi S}{2} - \frac{\pi S}{4} \end{bmatrix} + \frac{\pi S}{4} \begin{bmatrix} 1 \\ \vdots \\ 1 \end{bmatrix} \begin{bmatrix} 1 \\ \vdots \\ 1 \end{bmatrix}^T \right]^{-1} \quad (21)$$

Let $k = \frac{\pi S}{2}$. It follows directly from Sherman Morrison that the i -th and j -th entries of V_ϕ are given as

$$(V_\phi)_{ij} = \begin{cases} \frac{2}{k} - \frac{2}{k(S+1)} & i = j \\ -\frac{2}{k(S+1)} & i \neq j \end{cases} \quad (22)$$

$$(V_\phi)_{ii} = \frac{4}{\pi(S+1)} \quad (23)$$

We see that the diagonals are the same. Thus, we take the PTG estimate in terms of a single marginal ϕ_i . Substituting in the s^2 estimate s_N^2 and using the second assumption, we write the variance of marginal ϕ_i as

$$\text{Var}(\phi_i) = \frac{4s_N^2}{\pi(S+1)} \frac{S}{S-2} \quad (24)$$

$$= \frac{4s_N^2}{\pi \times S} \quad (25)$$

Thus, the *total* number of samples needed is

$$S = \frac{4s_N^2}{\bar{\pi} \times \text{Var}(\phi_i)} \quad (26)$$

Because our notion of feature importance uncertainty is in the form of a credible interval, we use the normal approximation of $\text{Var}(\phi_i)$ and write

$$S = \frac{4s_N^2}{\bar{\pi} \times \left[\frac{W}{\Phi^{-1}(\alpha)} \right]^2} \quad (27)$$

where W is the desired width, α is the desired confidence level, and $\Phi^{-1}(\alpha)$ is the two-tailed inverse normal CDF. Finally, we subtract the initial N samples. Thus, PTG is given as

$$PTG(W, \alpha, x) = \frac{4s_N^2}{\bar{\pi}_N \times \left[\frac{W}{\Phi^{-1}(\alpha)} \right]^2} - N \quad (28)$$

□

C.2 Proposition 3.1

We outline three claims in the proposition. Namely, (1) $\text{Var}(\phi) \rightarrow 0$ as $N \rightarrow \infty$ (2) the mean of ϕ is consistent and (3) $\text{Var}(\epsilon)$ converges to the bias of the local model as $N \rightarrow \infty$

Convergence of $\text{Var}(\phi)$ Recall the posterior distribution of ϕ given in equation 4. In equation 21, we see the on and off-diagonal elements of V_ϕ are given as $\frac{4}{\bar{\pi}(N+1)}$ and $-\frac{4}{\bar{\pi}N(N+1)}$ respectively (here replacing S with N to stay consistent with equation 4). Because we have $N \rightarrow \infty$, these values define V_ϕ due to the law of large numbers. Thus, as $N \rightarrow \infty$, V_ϕ goes to the null matrix and so does the uncertainty over ϕ .

Consistency of $\hat{\phi}$ Recall the mean of ϕ , denoted $\hat{\phi}$ given in equation 5. To establish consistency, we must show that $\hat{\phi}$ converges in probability to the true ϕ as $n \rightarrow \infty$. To avoid confusing true ϕ with the distribution over ϕ , we denote the true ϕ as ϕ^* . Thus, we must show $\hat{\phi} \rightarrow_p \phi^*$ as $n \rightarrow \infty$. We write

$$\hat{\phi} = (\mathcal{Z}^T \text{diag}(\Pi_x(\mathcal{Z}))\mathcal{Z} + I)^{-1} \mathcal{Z}^T \text{diag}(\Pi_x(\mathcal{Z}))Y \quad (29)$$

$$= (\mathcal{Z}^T \text{diag}(\Pi_x(\mathcal{Z}))\mathcal{Z} + I)^{-1} \mathcal{Z}^T \text{diag}(\Pi_x(\mathcal{Z}))(\mathcal{Z}\phi^* + \epsilon) \quad (30)$$

Considering the mean of ϵ is 0

$$= (\mathcal{Z}^T \text{diag}(\Pi_x(\mathcal{Z}))\mathcal{Z} + I)^{-1} \mathcal{Z}^T \text{diag}(\Pi_x(\mathcal{Z}))\mathcal{Z}\phi^* \quad (31)$$

Through the law of large numbers

$$= (n^{-1}[\mathcal{Z}^T \text{diag}(\Pi_x(\mathcal{Z}))\mathcal{Z} + I])^{-1} n^{-1} \mathcal{Z}^T \text{diag}(\Pi_x(\mathcal{Z}))\mathcal{Z}\phi^* \quad (32)$$

$$= \phi^* \quad (33)$$

which establishes the claim.

Convergence of $\text{Var}(\epsilon)$ Assume we have $N \rightarrow \infty$ so $\hat{\phi}$ converges to ϕ^* . The uncertainty over the additive error term is given as the variance of the distribution in equation 7. The variance of this generalized student’s t distribution is given as

$$s^2 \frac{N}{N-2} \quad (34)$$

which for large N is s^2 . Recalling the definition of s^2 (see equation 17), s^2 reduces to the local error of the model as $N \rightarrow \infty$, namely

$$s^2 = \frac{(y - \mathcal{Z}\hat{\phi})^T \text{diag}(\Pi_x(\mathcal{Z}))(y - \mathcal{Z}\hat{\phi})}{N} \quad (35)$$

which is equivalent to the squared bias of the local model, considering that there is no uncertainty over ϕ .

D Detailed Results

Quality of Uncertainty Estimates In section 4, we assessed whether our uncertainty estimates are well calibrated and presented results for BayesLIME and BayesSHAP. Here, we demonstrate that the BayesLIME uncertainty estimates capture the uncertainty within the original LIME framework. In Table 1, we show the results when we rerun LIME for each image using 10,000 perturbations and find the estimates to be similarly within the BayesLIME CI estimates. We cannot compute this for SHAP because the SHAP implementation does not randomly select perturbations.

Data set	Model	LIME % Within CI
ImageNet	VGG16	94.8
MNIST	CNN	97.2
COMPAS	Random Forest	97.6
German Credit	Random Forest	96.9

Table 1: We assess the credible interval estimates of BayesLIME by computing how often the true feature importance values for LIME falls within our 95% CI estimate. Though we cannot get a true feature importance estimate, we compute the feature importance at a very high sampling size (10,000 perturbations) and assess how often these values fall within the CIs of our explanations computed at 100 perturbations.

Explanation Error as a Metric of Explanation Quality In section 4, we evaluated whether $P(\epsilon = 0)$ is a better metric for explanation quality than locally weighted R^2 and showed results for BayesLIME. Here, we demonstrate similar results for BayesSHAP. SHAP does not support locally weighted R^2 , so we compare BayesSHAP ranked by $P(\epsilon = 0)$ with BayesSHAP ranked by local fidelity. We evaluate each image in the MNIST testing set, sweeping over a range of perturbation amounts ([100, 150, 200, 250, 300, 350, 400, 450, 500]) and assess $\Delta_{\text{class-probability}}$. The results in Figure 8 show a *negative* relationship between fidelity and $\Delta_{\text{class-probability}}$, and demonstrate a *positive* relationship between our metric and $\Delta_{\text{class-probability}}$. This may be because local fidelity does not account for perturbation sample size.

Correctness of the Estimated Number of Perturbations In section 4, we assessed if *PTG* produces good estimates of the number of additional samples needed to reach the desired level of feature importance certainty. In figure 9, we show the desired level of certainty (desired width of credible interval CI_w) versus the actual *PTG* estimate (i.e. the estimated number of perturbations) for figure 6 in the main paper. We see the estimated number of perturbations is highly variable depending on desired CI_w . For the lowest levels of certainty, *PTG* ranges from 200 to 5000 perturbations. For the highest levels of certainty considered, *PTG* ranges from 200 to 20000.

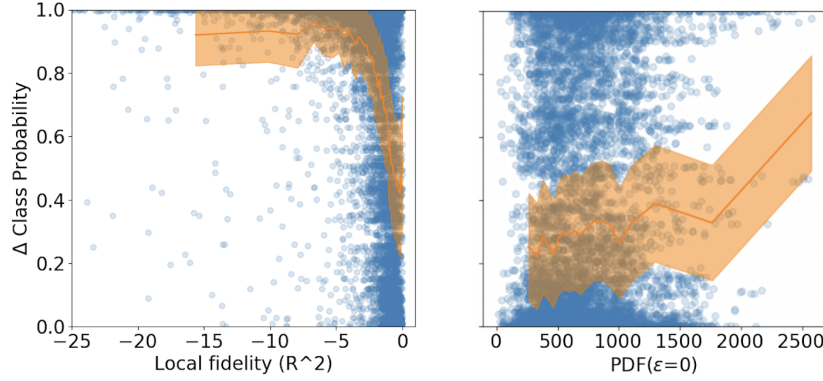


Figure 8: Δ class probability experiment from figure 5 repeated for BayesSHAP. The line provided is the mean and standard deviation of binned points. We see that our $\text{PDF}(\epsilon = 0)$ metric has a *positive relationship* with explanation quality as a measured by Δ class probability while fidelity has a *negative relationship*. The relationships are significant according to a Pearson’s correlation coefficient test ($p < 1e - 20$ in both cases). The local fidelity term for SHAP is very low because the resulting Shapley values tend to be extremely small or large, which can lead to poor locally weighted R^2 .

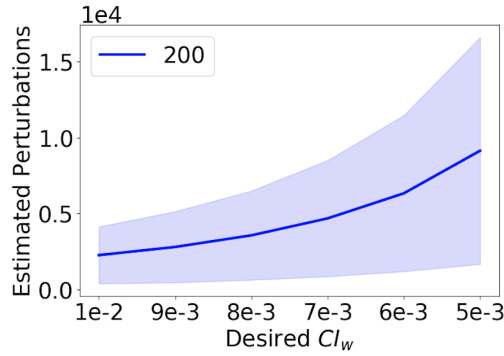


Figure 9: Desired CI_w versus the actual number of perturbations estimated by *PTG* in figure 6 of the main paper. We plot mean and standard deviation of *PTG*.

Efficiency of Uncertainty Sampling In section 4, we evaluated whether uncertainty sampling produces quicker convergence to high quality explanations and presented results plotting wall clock time versus $P(\epsilon = 0)$. In figure 10, we plot the number of model queries versus $P(\epsilon = 0)$. This experiment is analogous to figure 4 in the main paper, but here we use the number of model queries instead of time on the x-axis. We see that uncertainty sampling is more query efficient than random sampling for BayesLime.

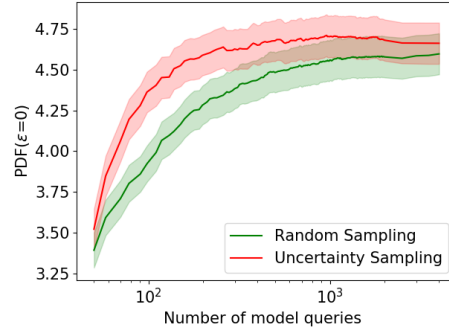


Figure 10: Assessment of the number of model queries needed to converge to a high quality explanation (analogous to figure 4 in the paper). We use both random sampling and uncertainty sampling over 100 Imagenet images. We provide the mean and standard error for binned estimates of these values.

E User study

In this appendix, we give an example screen shot from the user study.

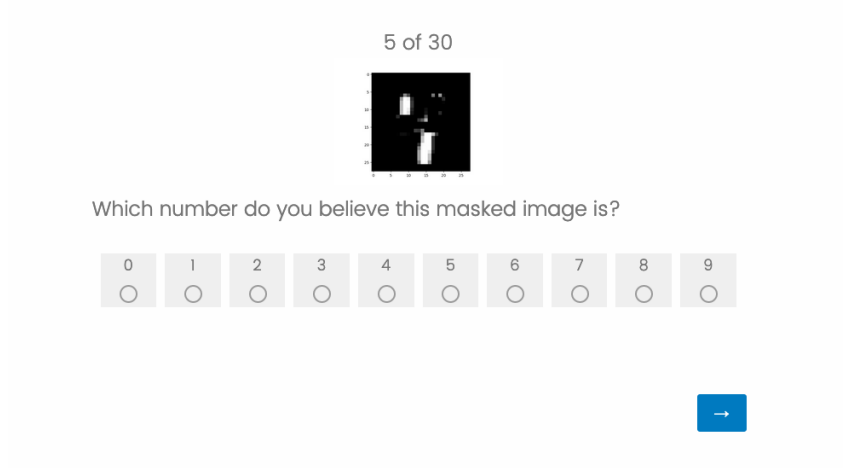


Figure 11: Screen shot from user study (correct answer 4).

F Uncertainty sampling algorithm

Here, we provide pseudo code for the uncertainty sampling procedure.

Algorithm 1 Uncertainty sampling for local explanations

Require: Perturbation size S , Preliminary perturbation size N , Batch size B , Model f , Data instance X , Explanation Model g with Predictive Variance ϕ_g , Candidate perturbation batch size \mathcal{A}

```

1: function UNCERTAINTY SAMPLE
2:   Initialize data set  $\mathcal{D}$  and add  $N$  initial perturbations,  $(\mathcal{Z}, f(\mathcal{Z}))$ .
3:   Fit  $g$  on  $\mathcal{D}$ 
4:   for  $i \leftarrow 1$  to  $S - N$  do
5:     if  $i \bmod B = 0$  then
6:       Generate set of candidate perturbations  $\mathcal{Q}$  of size  $\mathcal{A}$ 
7:       Draw  $B$  perturbations into  $\mathcal{Q}_{\text{new}}$  from  $\mathcal{Q}_{\text{dist}} \sim \exp(\phi_g(\mathcal{Q}))_{j \in |\mathcal{Q}|} / \sum \exp(\phi_g(\mathcal{Q}))$ 
8:        $\mathcal{D} \leftarrow \mathcal{D} \cup (\mathcal{Q}_{\text{new}}, f(\mathcal{Q}_{\text{new}}))$ ; Fit  $g$  on  $\mathcal{D}$ 
9:     end if
10:  end for
11:  return  $g$ 
12: end function

```
